A three-beam aerosol backscatter correlation lidar for wind profiling

Narasimha S. Prasad,[a,*] Anand Radhakrishnan Mylapore,[b]
[a] NASA Langley Research Center, 5 N. Dryden St., MS 468, Hampton, VA 23681
[b] Aeromancer Corporation 6992 Columbia Gateway Dr, Columbia, MD USA 21046

Abstract. In this paper, the development of a three-beam aerosol backscatter correlation (ABC) lidar to measure wind characteristics for wake vortex and plume tracking applications is discussed. This is a direct detection elastic lidar that uses three laser transceivers, operating at 1030 nm wavelength with ~10 kHz pulse repetition frequency and nanosec class pulse widths, to directly obtain three components of wind velocities. By tracking the motion of aerosol structures along and between three near-parallel laser beams, three-component wind speed profiles along the field-of-view of laser beams are obtained. With three 8-inch transceiver modules, placed in a near-parallel configuration on a two-axis pan-tilt scanner, the lidar measures wind speeds up to 2 km away. Optical flow algorithms have been adapted to obtain the movement of aerosol structures between the beams. Aerosol density fluctuations are cross-correlated between successive scans to obtain the displacements of the aerosol features along the three axes. Using the range resolved elastic backscatter data from each laser beam, which is scanned over the volume of interest, a 3D map of aerosol density in a short time span is generated. The performance of the ABC wind lidar prototype, validated using sonic anemometer measurements, is discussed.

Keywords: lidar, wind lidar, wind profiler, aircraft wake vortex, aerosol, velocimetry, turbulence, 3D winds

***First Author, E-mail: narasimha.s.prasad@nasa.gov

1 Introduction

Laser based remote sensing techniques, commonly known as Light Detection and Ranging (LIDAR) techniques, play a significant role in measuring wind characteristics for various applications [1-8]. Lidar techniques for nonintrusive sensing and profiling of wind velocities, in general, from an operational perspective can be classified based on laser type as CW or pulsed, and detection scheme such as direct detection or coherent detection. Each of these techniques has their own advantages and disadvantages, and their efficacy is based on adaptation of advances that are primarily being made in laser transmitter and receiver (transceiver) technologies. Lidar instrumentation coupled by effective data retrieval and processing algorithm tools help in data analysis as in the case of characterization of aircraft generated wake vortices. Besides transceiver instrumentation and algorithm tools, innovations in lidar system engineering

architecture contributes to their effective deployment in demanding circumstances, and from varied platforms including aircrafts, UAVs, and ships. Moreover, direct measurement of three velocity components from a compact system as opposed to indirect measurement, by extracting them from the line-of-sight velocity measurements, could simplify system complexity and further expand lidar advantages such as in plume tracking etc.

Compact and cost effective lidars with reduced complexity and enhanced portability for field deployment are required for measuring three component wind characteristics in diverse environments. Advances in operational techniques and component technologies are being sought for obtaining high-resolution time resolved wind information over desired ranges. Such measurements can be currently obtained with point sensors such as ultrasonic or hot-wire anemometers or with coherent Doppler lidars. The anemometers provide local information only while a Doppler lidar provides line-of-sight wind velocity profiles, and to obtain three-component wind profiles transmitted beam has to be scanned over large measurement cone angles. Current methods of non-intrusive airspeed measurement include techniques such as Laser Doppler Velocimetry (LDV), Particle Imaging Velocimetry (PIV) and Doppler Global Velocimetry (DGV), are better suited for wind tunnel use and are not practical for long-range, outdoor, standoff measurements. Therefore, architectural advances are needed for detection and tracking of aircraft wake vortices along glide slopes, measurement of turbulence intensity and wind shear profiles in space constrained environments such as inside wind tunnels, or from aircrafts and UAV platforms. Accordingly, lidars with reduced size, weight and power consumption (SWaP) as well as less complex configurations compared with Doppler coherent lidars are sought for obtaining wind velocity profiles which otherwise could not be obtained under realistic scenarios using current technologies. Multiple beam lidars and their application

to cross-wind measurements have been reported in the past [9-11]. In this paper, capitalizing on the advances being made in laser transceiver technologies and software algorithms, the development of an innovative, compact, eyesafe and direct detection aerosol backscatter correlation (ABC) lidar using three near-parallel laser beams for obtaining three component wind profiles is discussed. Here, wind velocities are measured using the ubiquitous airborne particulate aerosols that act as tracers of air motion. This technology development was initiated primarily for the detection and characterization of aircraft wake vortices. Besides measuring wake vortex characteristics and tracking plumes, the ABC lidar can be used as a remote velocimetry system for measuring three component concurrent winds profiles and turbulence. Such a system could be made as an integral part of wind tunnels, hover chambers and anechoic facilities to nonintrusively obtain three-component concurrent wind profiles to study key challenges in aerodynamics, aeroacoustics and flight dynamics. In addition to airspeed sensing, the proposed instrument could also have potential applications in spray characterization, aerosol transport and flow visualization. In Section 2, the architecture of the ABC lidar assembly and in Section 3, the salient features of wind retrieval algorithm for extraction of three component wind velocities are described. The results of field experiments are presented in Section 4, followed by summary and conclusions in Section 5.

2 The ABC Lidar Assembly

The ABC lidar system consists of three transceivers that transmit three near-parallel laser beams as shown in Figure 1. Each transceiver module consists of a laser module, detector, and telescope arrangement. The laser module, obtained from SESI, is a passively q-switched near-infrared Yb:YAG laser operating at 1030 nm that generate 12–18 ns wide pulses at high pulse repetition rate frequency (PRF) of about 10 KHz with a maximum average power of 3 W [12].

The pulsewidths were chosen to provide a spatial resolution of <3 m, with an ultimate goal of pulse duration as short as 7 ns for achieving a spatial resolution of 1 m. In addition, the laser output power satisfied our link budget analysis that suggested minimum pulse energy of ~100 μJ/pulse at a PRF of ~10 kHz to achieve acceptable signal to noise ratio of ≥ 2 at a range of 2 km, assuming an aerosol backscatter function of 1.82×10^{-6}/m/sr.

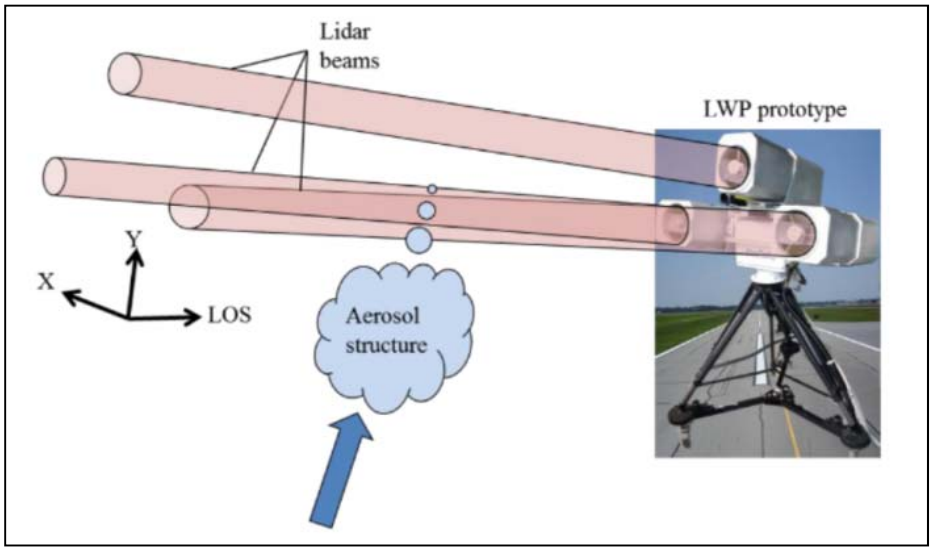

Figure 1. Illustration of the multi-beam lidar wind profiling approach using aerosol correlation.

A single-photon counting module (SPCM) detector, which is a Si-APD module from Excelitas (SPCM-AQRH) that has a maximum count rate of 20 MHz and a dead time of ~ 50 ns, is utilized. Yb:YAG lasers were selected since they offer a shorter wavelength (1030 nm) when compared with Nd:YAG (1064 nm) and Nd:YLF (1047 nm) lasers. As such, the quantum efficiency of Si-based SPCM detectors is higher with ~6% at 1030 nm than that at 1047 nm (~3%) and at 1064nm (~1%). The optics used for transmission and receiving the laser beams is an 8-inch diameter aperture telescope that transmits and receives the laser radiation along a narrow common field-of-view (FOV). The optical design of each transceiver is based on the early MicroPulse Lidar [13] and subsequent Portable Digital Lidar [14] designs in which the

transmitter and receiver share a focal plane field stop. The transmitter has a virtual stop that appears at the same distance and location as the physical receiver field stop. Referring to Figure 2, this is done by means of a Polarizing Beam Splitter (PBS) prism and a Quarter Wave Plate (QWP) located between the prism and the telescope. Horizontally polarized light from the IR laser is sampled for power normalization with an Energy Monitor (EM), then collimated with a small Beam Expander (BE), converted to vertical polarized light with a Half Wave Plate (HWP) so it will be totally reflected by the PBS into the transceiver telescope's Secondary Mirror (SM) and Primary Mirror (PM) to be transmitted to the atmosphere. A Negative Lens (NL) is used to f-match the beam to the transceiver telescope while creating a virtual field stop at exactly the same location as the Pin Hole (PH) field stop of the receiver as seen through an autocollimator. The outgoing light is circularly polarized by the QWP, and the backscattered return signal will be horizontally polarized after the second pass through the QWP so as to be nearly completely transmitted by the PBS. Light that exits the PH is collimated prior to transmitting through a Polarizer (PL) and a Narrowband Filter (NF) to reduce unwanted background light. Another positive lens focuses the light onto a solid-state single photon counting module Geiger mode Avalanche Photodiode (APD). The design of the transceiver was optimized to reduce internal scattering, which allows the instrument to detect aerosols as close as 15-20 m from the transceivers. The transceiver telescopes are focused at a distance of approximately 1.5 km in order to improve performance in the desired standoff range of less than 2 km.

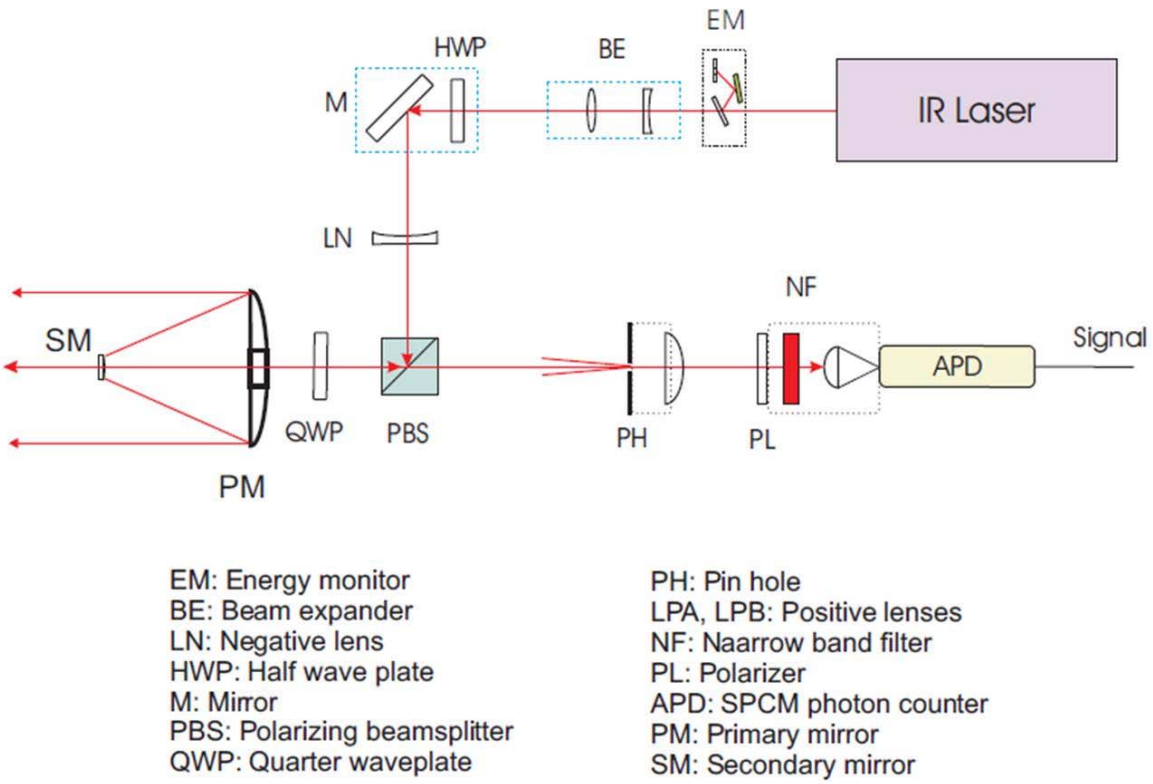

Figure 2. Optical schematic of the transceivers.

A multi-channel scaler (MCS) with 7.8 ns bins that provide ~1.2 m spatial resolution serves as the data acquisition system, and stores accumulated counts once every 50 ms to yield 20 profiles/sec. Although the MCS acquires the data at ~1.2 m spatial resolution, the laser pulse-width sets a lower bound of ~2 to 3 m on the effective spatial resolution of the system. The frame carrying the three transceivers is mounted on a computer controlled two axis pan-tilt scanner stage attached to a tripod. Two transceivers are mounted nearly parallel to each other along their side on the opposite side plates of the frame, while the third transceiver is mounted on the top plate in a triangular configuration as shown in Figure 3. Overall system azimuth and elevation pointing are made with the pan-tilt head on the tripod. The mechanical structure allows the

transceiver pointing angle to be adjusted along a single axis. The laser system requires 120VAC, 15A outlet for its operation.

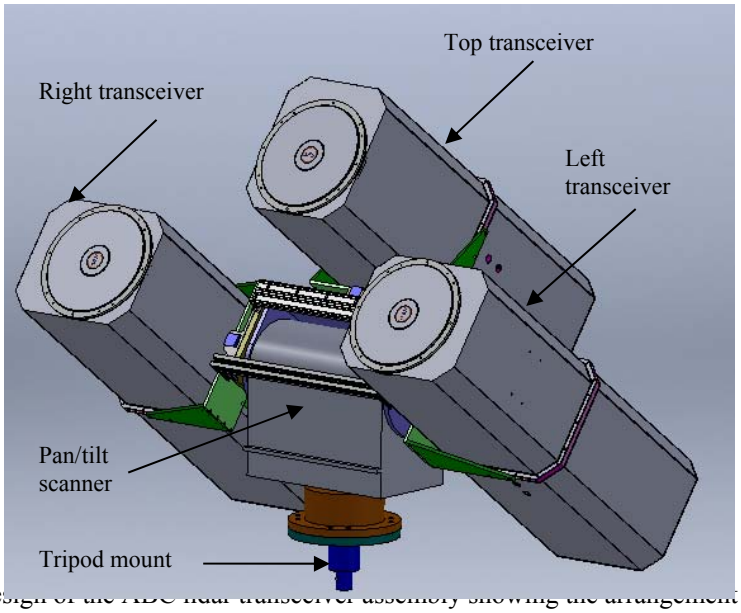

Figure 3. Design of the ABC lidar transceiver assembly showing the arrangement of three 8-inch aperture lidar transceivers on a common frame mounted on a pan-tilt scanner.

The ABC lidar system block diagram is shown in Figure 4. An electronics rack mount enclosure, separate from the three transceiver assembly, houses several electronics and ancillary components including the data system, the power supply, a chiller and a pan/tilt controller. The data acquisition system consists of a single-board computer (SBC) that houses a MCS for retrieving lidar signals; and USB Analog to Digital Converter (ADC) and Digital to Analog

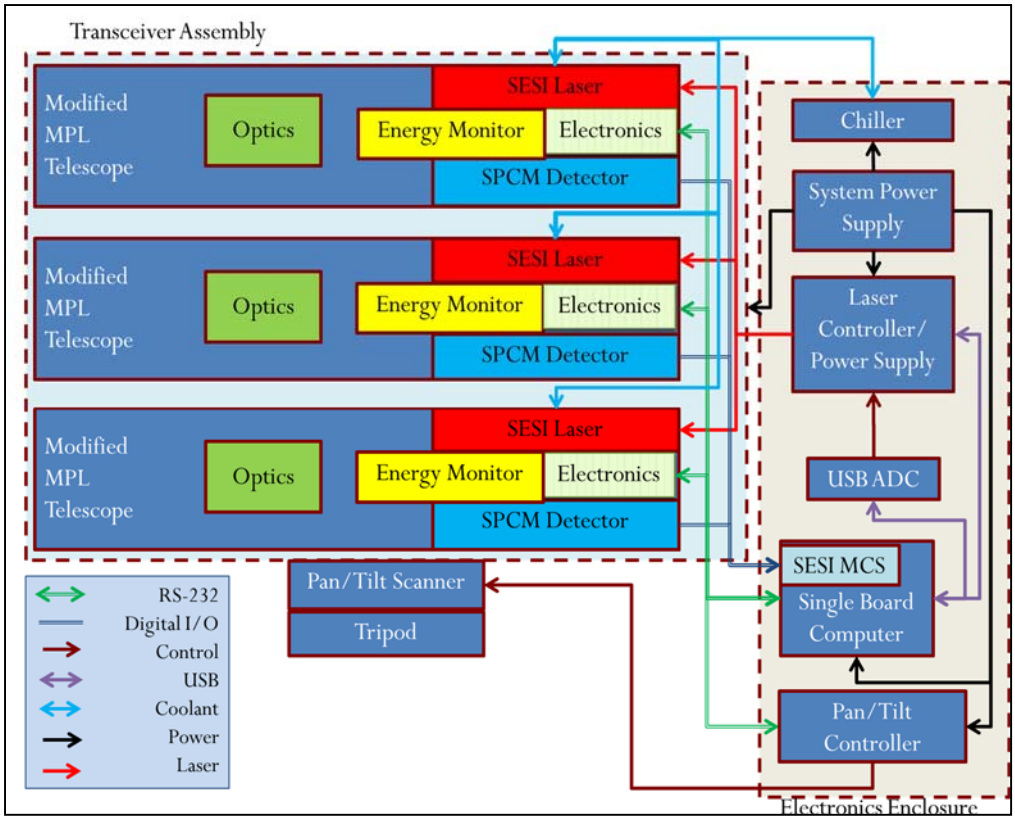

Figure 4. The ABC lidar system block diagram.

Converter (DAC) modules. A cable assembly carries the power, data, control and coolant lines from the electronics enclosure to the transceiver assembly and pan/tilt scanner.

The electronics enclosure is a shock mount standard 19 inch rack enclosure that houses the following major sub-systems: (a) Data Acquisition System, (b) Laser Control Box (LCB), (c) Pan/Tilt Controller, and (d) Chiller module.

(a) Data Acquisition System (DAC): The DAQ consists of an industrial PC chassis that contains a PCI/ISA bus backplane to accommodate the Single Board Computer (SBC) and peripherals, a hard drive for storage and cooling fans. A SBC, model CPGK CQ-26-X running Windows 7 is used to control the lidar. A 4-port RS-232 board is used to communicate with the laser and the pan/tilt controller. The lidar signal data acquisition board is a SESI model MCS-104 mounted on

a PC-104 to ISA bus adapter board. A National Instruments USD ADC board is used to read the orientation of the pan/tilt unit and also to send digital signals to enable the lasers.

(b) The laser control box (LCB): The LCB is a rack-mountable unit that can power and control as many as 3 lasers. The LCB also includes a USB digital-analog converter (DAC) module that outputs the voltage signal for each laser that sets the current of the pump diodes and therefore the output power of the laser. The flow sensor controls a timed relay that operates on a 10-second delay for turning the power to the unit on and off.

(c) Pan/tilt controller: A controller module for the pan/tilt unit provides AC signals for adjusting the pan and tilt positions. This controller communicates with the SBC over RS-232 and also provides analog voltage outputs for pan/tilt position feedback to the ADC. The controller is capable of moving the pan/tilt to programmable preset positions and scanning along the pan axis. Scanning along the tilt axis is implemented through software control from the SBC.

(d) ***Chiller Module:*** A rack mount chiller module provides coolant to the laser head and pump diodes in the transceivers. The chiller has an electronic controller for setting and monitoring the temperature. A flow sensor in the chiller module is used as a safety feature that prevents the LCB from powering on if the coolant flow is not active.

Auxiliary sensors for monitoring important variables include; (a) four thermistors for monitoring the temperature of the laser head, laser chill-plate, the transceiver main plate, the detector and in the thermo-electric cooler that controls the laser base plate temperature, (b) Laser power monitor sensor in the transmit optics consisting of a photodiode, (c) a two-axis inclinometer for sensing the orientation of the transceiver and a trigger circuit for sensing the laser pulse, which converts the output of a photodiode inside the laser head into a trigger pulse for synchronizing the laser with the MCS data acquisition and a transceiver control board (TCB),

which includes circuitry for powering the transceiver, monitoring the state variables and controlling and monitoring the detector power supply by communicating with the SBC over an RS-232 connection (d) an ethernet camera with enhanced sensitivity in the Near-IR (NIR) laser wavelength of 1030 nm that functions as a scope and aids in pointing, alignment and calibration of three transmit beams when used with a reflective target board or similar apparatus. The photodiode, which serves as an optical pickup to provide a trigger pulse to the MCS when the laser pulse is emitted, is required as the laser is passively Q-switched and the repetition rate tends to fluctuate with time. Figure 5 shows the completely assembled lidar mounted on a truck.

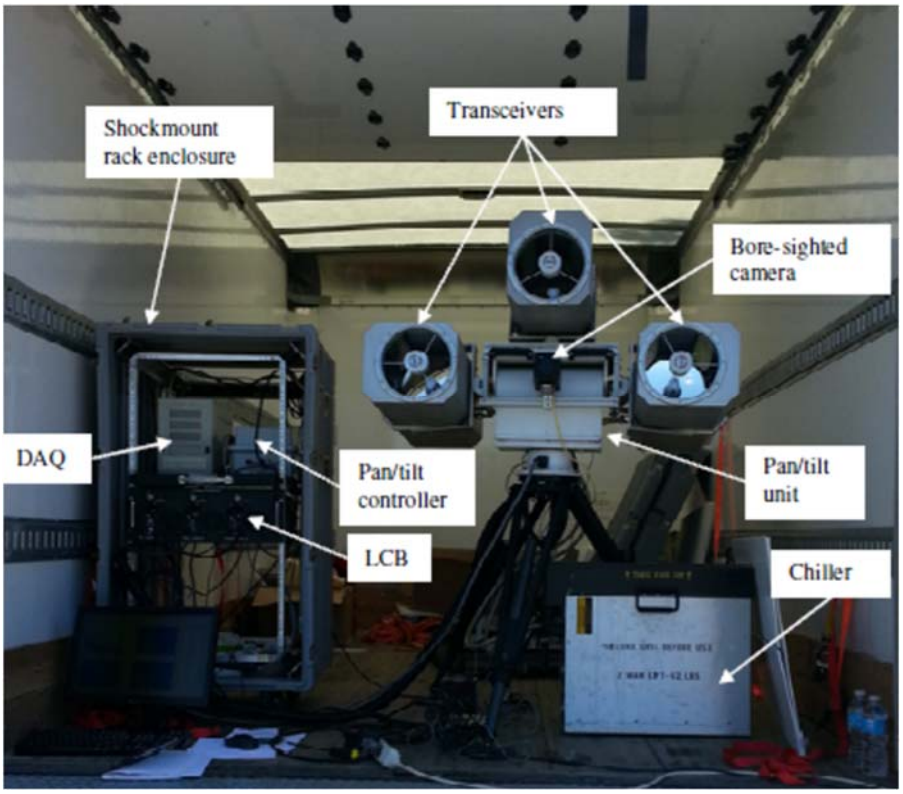

Figure 5. The ABC lidar system showing tripod mounted transceiver and electronics enclosure.

3 Wind Retrieval Algorithm

The wind retrieval algorithm utilizes the movement of aerosols through two closely spaced laser beams by observing the shift in the backscatter signals between the two beams [15-17]. It is similar to the methods of Piironen and Eloranta (1995), Mayor and Eloranta (2001), and Buttler et. al. (2001). Their algorithms were developed for retrieving 2-D vector winds from scanning, volume imaging lidars. They utilize a time series of 2-D (latitude vs. longitude) arrays of aerosol backscatter data taken with a horizontal scan. Our problem is somewhat simpler in that we only need to derive a single line of wind vectors at points along a 1-D (range) horizontal path. We retrieve wind data from just three closely spaced near-parallel LOS measurements. The basic algorithm for deriving the wind profiles from the aerosol backscatter profiles was described in Ref 24 as outlined below:

1. Lidar aerosol backscatter profiles are recorded from the three lidar channels and normalized by the laser power.
2. The signal fluctuations from aerosol structures are extracted from the profiles by eliminating the background signal, which includes Rayleigh scattering, uniformly mixed aerosol scattering and stationary objects such as vegetation.
3. Each 2-D (range vs. time) signal array is then low pass filtered in time and space to reduce random noise.
4. The pre-processed image arrays from each pair of lidar channels (i,j) are then sent through an optical flow calculation algorithm to obtain the range ($\Delta r_{i,j}$) and time ($\Delta t_{i,j}$) shift at each pixel.

5. The LOS wind component is determined from the ratio of the range and time shifts, $LOS_{i,j} = \frac{\Delta r_{i,j}}{\Delta t_{i,j}}$

6. The cross-wind $X_{i,j}$ at each range R is the spatial separation of the beams divided by the time-lag at that range. $X_{i,j} = \frac{a_{i,j} + R\sin(\theta_{i,j})}{\Delta t_{i,j}}$, where $a_{i,j}$ is the separation distance between the beams at origin and $\theta_{i,j}$ is the separation angle between the two lidar beams.

7. The LOS and cross-wind components from the three pairs of channels are then combined vectorially to produce the three components of wind speed: LOS, X and Y. Here, LOS is the wind speed component towards the lidar along the beam LOS; X-wind is the horizontal wind component from left to right; and Y-wind is the vertical wind component referenced from the bottom to the top orthogonal to the three beams (Figure 6).

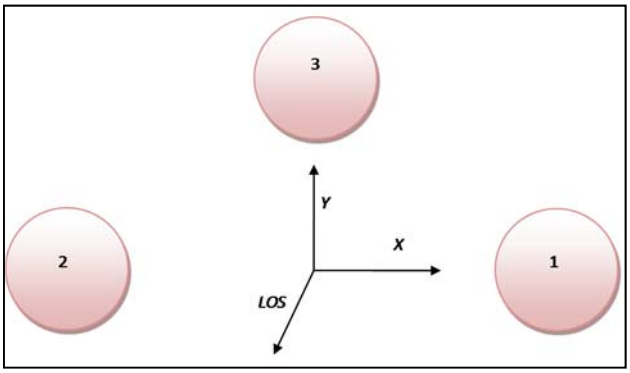

Figure 6. Illustration of the three wind components in reference to the three beams.

4 Experimental Tests

The pulsed lidar beams scatter off of aerosol particles that are ever-present in the lowest levels of the atmosphere, the boundary layer. Fluctuations in the density of aerosols show up as persistent aerosol features in the lidar signals that drift with the speed and direction of the wind.

These fluctuating signals at each range along one beam can be cross-correlated with the signals along the other beam to measure cross wind, or with adjacent range bins in each individual beam to measure Line-of-Sight (LOS) wind. A third beam placed above or below the other two in elevation enables vertical winds to also be measured as a function of range. This technique is analogous to the way hot-wire and sonic anemometers work to derive wind speed and direction in a small volume of air by cross-correlating the signals from three point sensors. For the lidars, each range bin along each beam acts like a single detector picking up the fluctuating atmospheric signals. These lidar bins can be grouped and cross-correlated to measure a 3-D wind vector. In this way, many wind vector measurements along a LOS are possible using a multi-beam aerosol scattering lidar (see Refs 10 and 11). The big advantage of an aerosol correlation lidar approach is its ability to make accurate and independent wind measurements at small range increments over the entire range on short time scales. Wind profiles along various linear segments of the flow can simply be obtained by scanning the lidar through the flow volume. The lidar backscatter images from each pair of beams are cross-correlated using optical flow algorithms to find the aerosol displacements in space and time, which are used to derive two-component airspeed maps. The three sets of two-component airspeed maps are combined vectorially to produce the three components.

Preliminary field tests have been conducted using this prototype system at various locations ranging from Columbia, MD, the Howard University Beltsville Research Site located in Beltsville, MD and at NASA Langley Research Center (LaRC). Results of tests conducted using this prototype in Columbia and Beltsville Research Site locations in Maryland has yielded promising results and has been discussed in Ref [24]. The data from these tests shows that the multiple beam lidar is capable of measuring winds accurately even during gusty, turbulent

conditions. One test of this prototype system, which was presented in Ref [24] was conducted on January 21, 2014 in Columbia, MD for just over an hour in a snowstorm featuring moderate snowfall with wind gusts up to 10 m/s. The prototype system was located inside the building and pointed out of a loading dock at a small hill about 50m away, where an RM Young 81000 three-axis sonic anemometer was set up to acquire measurements at a 20 Hz sampling rate. The lidar backscatter plots show strong elastic return from the snowfall and aerosol structures, with the slope of the structures indicating strong and quite turbulent wind fields. Figure 7 shows the comparison of the three-axis LWP wind measurements with the sonic anemometer measurements from the test, where the mean ("mean diff") and RMS difference ("RMS diff") between the LWP and the anemometer measurements is provided along with the standard deviation of the sonic anemometer data ("sonic std. dev.") for each axis. These plots clearly show that the lidar wind measurements track very closely with the changes in wind measurements from the anemometer. The RMS difference between the lidar and sonic anemometer measurements is on the order of 1 m/s and the mean difference is less than 1 m/s. The RMS difference is found to be closely related to the standard deviation of the sonic anemometer measurements. The mean of the lidar X-wind measurements was found to be slightly higher than the sonic anemometer measurements, which might be related to the fact that the lidar measurement volume was approximately 2m above the anemometer. The data from these tests shows that the lidar is capable of measuring winds accurately even during gusty, turbulent conditions.

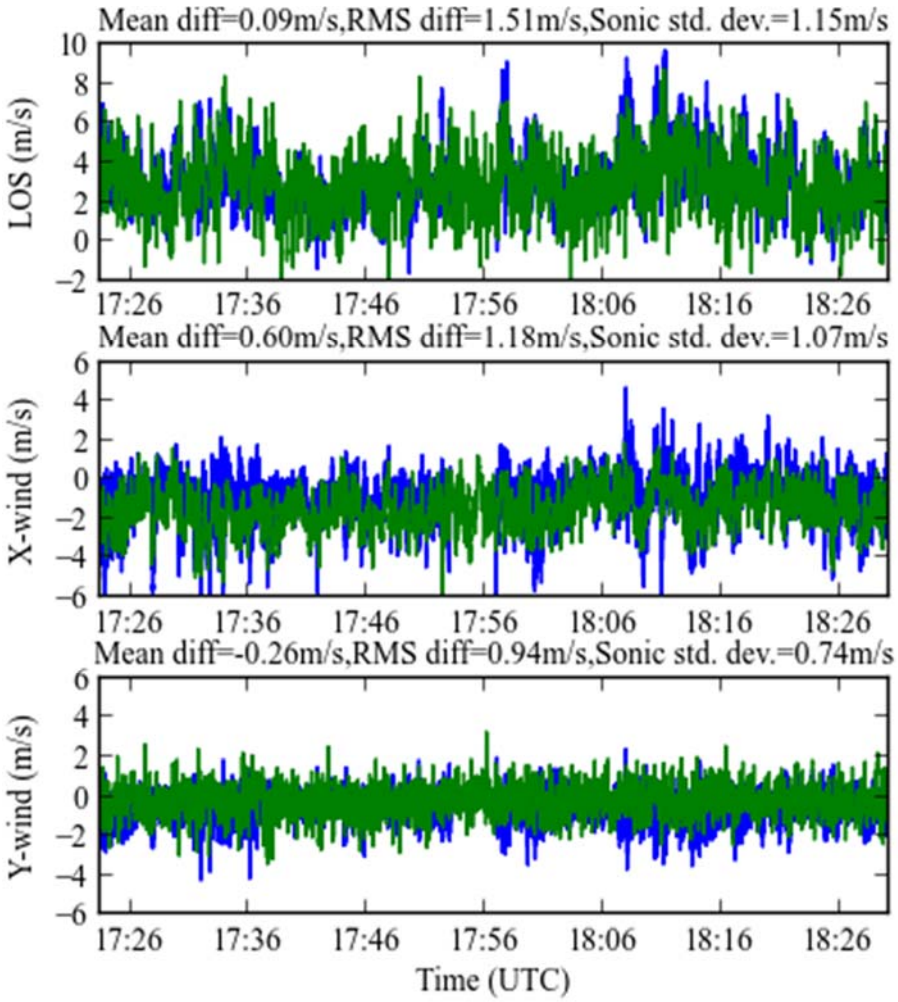

Figure 7. Three components of lidar wind speed (green line) compared with the sonic anemometer (blue line) from tests conducted on January 21, 2014. The sampling rate of both lidar and anemometer measurements is 20 Hz. The lidar wind data was calculated using a 5x5 bin interrogation window and filtered using a 15 range bins x 61 time bins Gaussian smoothing window.

In this section, field experiments conducted at NASA LaRC test site are presented. The ABC lidar, installed inside a covered laboratory with large doors, transmitted three lidar beams out over a long field (see Figure 8). The separation distance of the three lidar beams was calibrated by pointing the instrument at a target board with a special reflective sheet that enhanced the reflection of the lidar beams along the same path. The detectors were turned off in order to protect them from being damaged by the large optical signal reflected by the target board. The IR camera was used to image the reflection of the beams on the target board, which was then analyzed to calculate the relative beam divergence angles of the beams with respect to each

other. A RM Young Model 61000 ultrasonic anemometer was placed along the LOS of the ABC lidar at a distance of approximately 15 m from the lidar system. The atmospheric conditions on this day were extremely clear, with very few aerosols visible in the lidar backscatter measurements. Therefore, in order to seed the flow, two small theatrical fog machines were installed about 30 m away from the wind lidar along the LOS as the prevailing wind was predominantly directed towards the lidar. The image captured by the IR camera as it looked over the field is shown in the top left picture in Figure 8, and shows the anemometer and the fog machine. The view looking towards the lidar is shown in the right picture in Figure 8. This

Figure 8. Pictures showing experimental layout at NASA LaRC test site on December 9, 2015. Left picture: The ABC lidar system on a tripod and electronics enclosure located inside a building. Middle picture: The lidar system is shown in the background, and the sonic anemometer and a fog machine visible in the foreground. Right pictures: Top picture shows the test range with sonic anemometer and the bottom picture shows three lidar beams visible on a reflective target board at a distance of 140 m. The pictures in the right are captured by the IR camera located on the lidar system.

configuration was chosen so that the point at which the fog clouds intersected the lidar beams was located approximately in the vicinity of the anemometer. A sample four-minute set of lidar backscatter data from this test is shown in Figure 9, where the lidar backscatter data shows the fog releases, which are moving along with the prevailing wind towards the lidar.

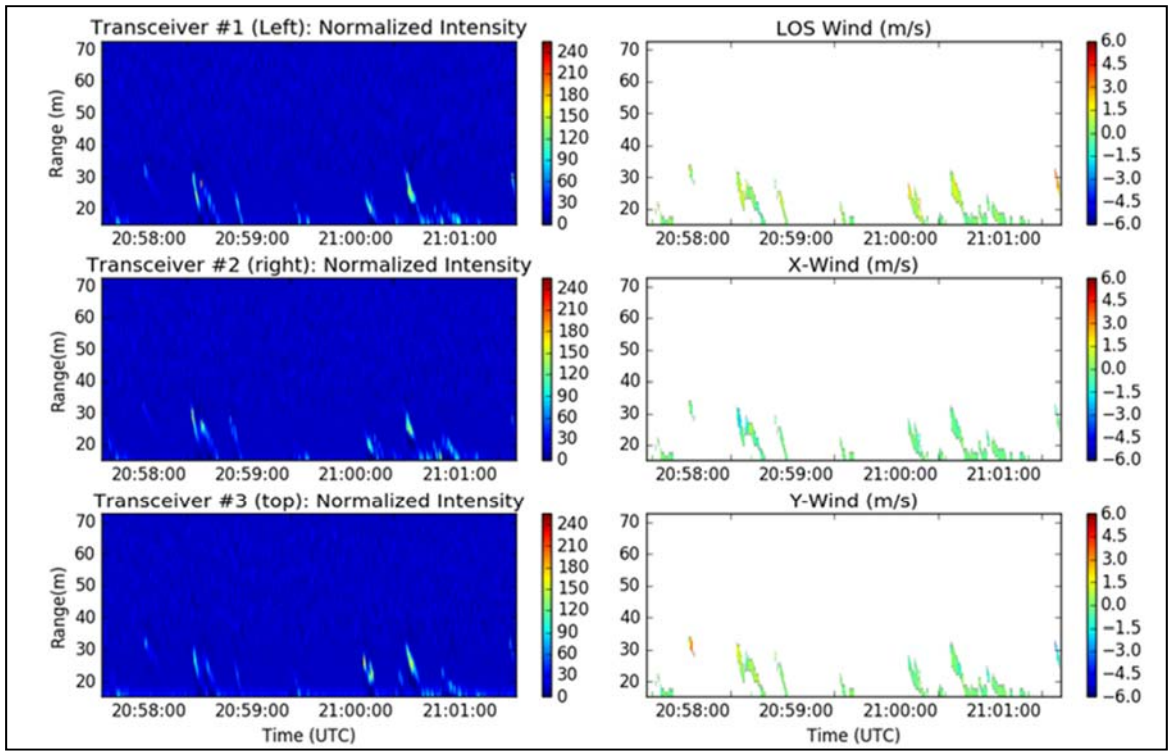

Figure 9. Four minute set of test data from the experiment conducted at NASA LaRC on December 9, 2015 using the LWP Prototype. The left plots show pre-processed lidar backscatter data from the 3 channels, where fog releases are visible as streaks moving towards the lidar. The right plots show the 3 airspeed components, reported every 1.17m in range reported at a 20 Hz rate in time.

Preliminary analysis of this lidar data with the 2D false color plot of extracted airspeeds along the three components is also shown Figure 9. These lidar airspeed measurements were compared with data from the ultrasonic anemometer and are shown in Figure 10. Over two hours of data were obtained with periodic seeding by the fog machine. Because the wind direction was towards the lidar, the region of seeding was restricted to a small region from the lidar dead zone (15 m from the lidar) to where the fog entered the lidar FOV. In spite of this challenge, the lidar measurements of airspeed agree very well with the anemometer measurements in all three

components. The difference in the mean values of the lidar and sonic anemometer measurements were negligible and the RMS difference between the measurements was < 1 m/s and compared well with the standard deviation of the airspeeds. In addition to the data obtained from staring along a single LOS, 30 minutes of data was obtained by scanning the three-beam lidar assembly

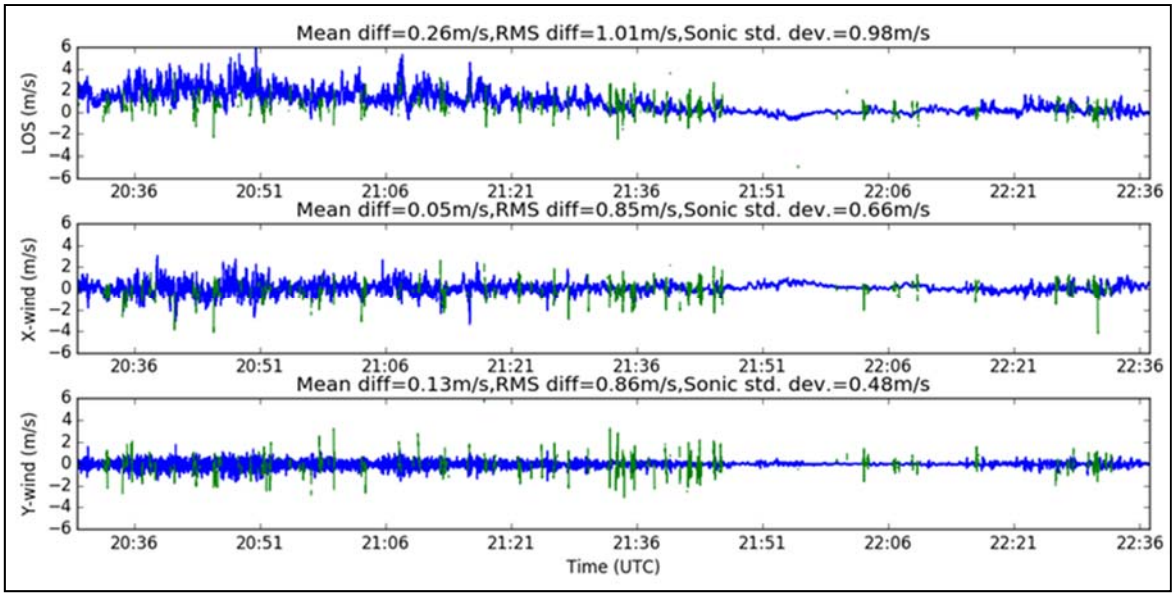

Figure 10. Three components of lidar wind speed (green line) compared with the sonic anemometer (blue line) from over 2 hours of measurements on December 9, 2015. The sampling rate of both lidar and anemometer measurements is 20 Hz. The lidar wind data was calculated using a 5x5 bin interrogation window and filtered using a 21 range bins x 51 time bins Gaussian window.

along the horizontal scan axis. Table 1 shows the current ABC lidar system specifications. Currently, efforts are underway to refine the system architecture and retrieval algorithms to further reduce SWaP and increase velocity resolution.

Table 1. The ABC lidar specifications

Measurement Characteristics	Specifications
Wavelength	1030 nm
Pulsewidth	12-18 ns
PRF	~10 kHz
Telescope Aperture Diameter	8 inches
Horizontal Wind Range (min, max)	0-30 m/s
Range	20 m – 2 km
Wind Error	< 0.5 m/s (mean)
Wind Profile Range Resolution	1.2 m
Wind Profile Update Time	0.05 sec
Eye Safety	ANSI Z-136.6-Cllass 1M

5 Summary and Conclusions

In this paper, the development of a three-beam aerosol backscatter correlation (ABC) lidar for wind profiling is discussed. This is a direct detection, short-pulsed wind lidar mounted on a tripod that provides three components of wind velocities along the LOS. Performance validation tests carried out at NASA Langley Research Center and other places have shown the difference in the mean values of the ABC lidar and sonic anemometer measurements were negligible and the RMS difference between the measurements was < 1 m/s. Using this system, further tests under a broad range of test conditions are being planned. Furthermore, advances to the current first-of-a-kind prototype are being looked into for reducing the SWaP and by incorporating scanning mode capability in place of pan/tilt scanner. In addition, advanced algorithms for characterizing 3D winds for wake vortex and other applications under the full range of anticipated atmospheric conditions is being investigated. Measuring 3D wind speeds along a LOS as a function of range and time has several applications including characterizing aircraft wake vortices and plume tracking. Other applications for which the technology is being investigated include the non-intrusive measurement of 3D global airspeeds inside a wind tunnel

by tracking aerosol structures moving through the test section using high-resolution lidar backscatter measurements from a laser beam scanned rapidly over the measurement volume. Also, this technology can be expanded to function as a 3D range-finder both for static and dynamic applications. 3D ranging coupled with turbulence measurements would help in obtaining solid boundary maps of objects in the wind tunnel from the lidar backscatter and airspeed data.

Acknowledgements

The authors gratefully acknowledge funding under the following contracts: a NASA SBIR Phase II program entitled, Lidar Wind Profiler for the NextGen Airportal, contract No. NNX11CB72C; and a NAVAIR SBIR Phase II program entitled, Aerosol Lidar Velocimeter for Rotorcraft Downwash Measurements, N68335-12-C-0136. We would also like to thank Susan Polsky of NAVAIR for her support.

References

1. Albrecht, H., Borys, M., Damaschke, N., and Tropea, C. *"Laser Doppler and Phase Doppler Measurement Techniques,"* Eds. R. Adrian, M. Gharib, W. Merzkirch, D. Rockwell, and J. Whitelaw. Springer-Verlag, Berlin (2003).
2. Prasad, Ajay K. "*Stereoscopic particle image velocimetry"* Experiments in fluids 29.2, 103-116 (2000).
3. Derr, V. E. and Little, C. G., *"A Comparison of Remote Sensing of the Clear Atmosphere by Optical, Radio, and Acoustic Radar Techniques,"* Appl. Opt. **9**, 1982–1983, 1970.

4. Zuev, V. E., Zadde, G. O., Tarasenko, V. P., and Yurga, N. I., *"Lidar Sounding of the Atmosphere to Estimate Static and Dynamic characteristics of Aerosol Inhomogeneities",* Proc., 5th Conference on Laser Radar Studies of the Atmosphere, Williamsburg, VA, pp. 104–105, 1973.
5. Eloranta, E. W., J. M. King, and J. A. Weinman, *"The Determination of Wind Speeds in the Boundary Layer by Monostatic Lidar,"* J. Appl. Meteor., **14**, 1485-1489, 1975.
6. Leuthner, T. G. and Eloranta, E. W., *"Remote Measurement of Longitudinal and Cross-Path Wind Velocities with a Monostatic Lidar,*" 8th International Laser Radar Conference, Philadelphia, PA., 1977.
7. Kunkel, K. E., Eloranta, E. W., and Weinman, J. A., *"Remote Determination of Winds, Turbulence Spectra, and Energy Dissipation Rates in the Boundary Layer from Lidar Measurements,"* J. Atmospheric Sciences, **37**, 1980.
8. Stull, R. B., *"An Introduction to Boundary Layer Meteorology,"* Kluwer Academic Publishers, p.32, 1988.
9. Schwemmer, G., D. O. Miller, T. D. Wilkerson, *"HARLIE aerosol and cloud structure and wind observations during HARGLO and IHOP," 6th International Symposium on Tropospheric Profiling: Needs and Technologies,* Leipzig, Germany, 14–20 September 2003, Institute for Tropospheric Research, Leipzig, Germany, pub., pp. 65-67 (2003).
10. Schwemmer, G.K., Banta, M., Achey, A., Lee, S., Mehta, N., Yakshin, M. and Blango, J., *"Wind Fields Measured Using Multi-Beam Commercial Aerosol Lidar,"* 25th International Laser Radar Conference, St. Petersburg, Russia, 281-284 (2010).
11. Schwemmer, G.K., Banta, M., Achey, A., Lee, S., Lei, J., Yakshin, M. and Blango, J., *"Cross-wind lidar prototype,*" *26th International Laser Radar Conference, Porto Heli, Greece*, 763-766 (2012).
12. Yakshin, M A. Fromzel, V A. and Prasad C. R. *"Compact, High Brightness and High Repetition Rate Side-Diode-Pumped Yb:YAG Laser"* Advances in Solid-State Lasers: Development and Applications, Book edited by: Mikhail Grishin, ISBN 978-953-7619-80-0, pp. 126-142, February 2010, INTECH, Croatia.

13. Campbell, J., et al., "Full-Time, Eye-Safe Cloud and Aerosol Lidar Observation at Atmospheric Radiation Measurement Program Sites: Instruments and Data Processing," *J. Atmos. Ocean Tech.*, 19, pp. 431-442, April 2002.
14. USPatent 6593582 B2, "Portable Digital Lidar", H.S.Lee, I.H.Hwang and C.R.Prasad, 2003
15. Piironen, A. K., and E. W. Eloranta, *"Analysis of wind profiles calculated from volume imaging lidar data," J. Geophys. Research*, **100**, D12, 25559-25567, 1995.
16. Mayor, S. D. and Eloranta, E. W., *"Two-Dimensional Vector Wind Fields from Volume Imaging Lidar Data," J. Appl. Meteor.*, **40**, 1331-1346, 2001.
17. Buttler, W. T., C. Soriano, J. M. Baldasano and G. H. Nickel, *"Remote Sensing Of Three-Dimensional Winds with Elastic Lidar: Explanation Of Maximum Cross-Correlation Method," Boundary-Layer Meteorology*, **101**, 305–328, 2001.
18. Prieur, J.L. , R. Avila, G. Daigne, and J. Vernin, *"Automatic Determination of Wind Profiles with Generalized SCIDAR," Publications of the Astronomical Society of the Pacific*, **116**, 778–789, 2004.
19. Farneback, G., *"Two-frame motion estimation based on polynomial expansion,"* Lecture Notes in Computer Science, 2749, 363-370 (2003).
20. Bradski, G. and Kaehler, A., [*Learning OpenCV: Computer Vision with the OpenCV Library*]. O'Reilly Media, (2008).
21. Liu, C., Beyond Pixels: *"Exploring New Representations and Applications for Motion Analysis,"* Doctoral Thesis. Massachusetts Institute of Technology. May 2009.
22. Danudibroto, A., Gerard, O., Alessandrini, M., Mirea, O., D'hooge, J., & Samset, E. *"3D Farnebäck Optic Flow for Extended Field of View of Echocardiography,"* Functional Imaging and Modeling of the Heart (pp. 129-136). Springer International Publishing (2015).
23. Hermann, S., & Werner, R., "High accuracy optical flow for 3D medical image registration using the census cost function," In *Image and Video Technology* (pp. 23-35). Springer Berlin Heidelberg (2014).

24. Radhakrishnan, A. et al.,*"A three-beam aerosol backscatter correlation lidar for three-component wind profiling "*, Proc. SPIE 9080, Laser Radar Technology and Applications XIX; and Atmospheric Propagation XI, 90800Y (June 9, 2014).

Caption List

Fig. 1 Illustration of the multi-beam lidar wind profiling approach using aerosol correlation.

Fig. 2 Figure 2. Design of the ABC lidar transceiver assembly showing the arrangement of three 8-inch aperture lidar transceivers on a common frame mounted on a pan-tilt scanner.

Fig. 3 The ABS lidar system block diagram.

Fig. 4 The ABC lidar system showing tripod mounted transceiver and electronics enclosure.

Fig. 5 Illustration of the three wind components in reference to the three beams.

Fig. 6 Pictures showing experimental layout at NASA LaRC test site on December 9, 2015. Left picture: The ABC lidar system on a tripod and electronics enclosure located inside a building. Middle picture: The lidar system is shown in the background, and the sonic anemometer and a fog machine visible in the foreground. Right pictures: Top picture shows the test range with sonic anemometer and the bottom picture shows three lidar beams visible on a reflective target board at a distance of 140 m. The pictures in the right are captured by the IR camera located on the lidar system.

Fig. 7 Four minute set of test data from the experiment conducted at NASA LaRC on December 9, 2015 using the LWP Prototype. The left plots show pre-processed lidar backscatter data from

the 3 channels, where fog releases are visible as streaks moving towards the lidar. The right plots show the 3 airspeed components, reported every 1.17m in range reported at a 20 Hz rate in time.

Fig. 8 Three components of lidar wind speed (green line) compared with the sonic anemometer (blue line) from over 2 hours of measurements on December 9, 2015. The sampling rate of both lidar and anemometer measurements is 20 Hz. The lidar wind data was calculated using a 5x5 bin interrogation window and filtered using a 21 range bins x 51 time bins Gaussian window.

Figure 9. Four minute set of test data from the experiment conducted at NASA LaRC on December 9, 2015 using the LWP Prototype. The left plots show pre-processed lidar backscatter data from the 3 channels, where fog releases are visible as streaks moving towards the lidar. The right plots show the 3 airspeed components, reported every 1.17m in range reported at a 20 Hz rate in time.

Figure 10. Three components of lidar wind speed (green line) compared with the sonic anemometer (blue line) from over 2 hours of measurements on December 9, 2015. The sampling rate of both lidar and anemometer measurements is 20 Hz. The lidar wind data was calculated using a 5x5 bin interrogation window and filtered using a 21 range bins x 51 time bins Gaussian window.

Table 1 The ABC lidar specifications